# Influence of Ammonia Annealing on Cr–N Thin Films and Their Thermoelectric Properties

Victor Hjort, Franck Tessier, Fabien Giovannelli, Arnaud Le Febvrier, Per Eklund

ACS APPLIED ENERGY MATERIALS



www.acsaem.org
Article

# Influence of Ammonia Annealing on Cr−N Thin Films and Their Thermoelectric Properties

Victor Hjort,* Franck Tessier, Fabien Giovannelli, Arnaud le Febvrier, and Per Eklund

Cite This: ACS Appl. Energy Mater. 2024, 7, 6785−6792
Read Online



**ABSTRACT:** CrN-based thin films are emerging as thermoelectric materials for energy harvesting. Their thermoelectric properties depend on phase composition and stoichiometry, necessitating control over the nitrogen content and how it affects the phase composition. Here, the effect of high-temperature ammonia annealing on the thermoelectric properties as well as crystal structure of thin films of Cr−N on *c*-plane sapphire ($Al_2O_3(0001)$) was investigated. Single-phase (cubic CrN) and mix-phase (cubic CrN + hexagonal-$Cr_2N$) Cr−N films were annealed in ammonia, converting any secondary phase of hexagonal $Cr_2N$ to cubic CrN. The thermoelectric properties of the films that contained a secondary phase of hexagonal $Cr_2N$ greatly improved upon annealing, with an increase of 900% to $0.5 \times 10^{-3}$ W m$^{-1}$ K$^{-2}$ for the film annealed at 800 °C for 2 h. Annealing of single-phase films of cubic CrN resulted in films with near-insulating electrical properties. For the thermoelectric applications of CrN, ammonia annealing can be beneficial over meticulous deposition control.

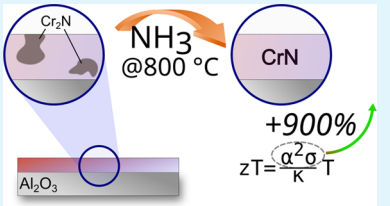


**KEYWORDS:** *CrN, thermoelectrics, thin film, ammonia, annealing, chromium*



## INTRODUCTION

Thermoelectric (TE) devices can convert heat to electricity (Seebeck effect), and vice versa (Peltier effect) without moving parts and with high reliability.[1−3] In TE devices, a current or voltage is generated as heat transports electrons or holes from the hot side to the cold side. Heat-to-electricity conversion could allow for harvesting of waste heat by TE generators, and Peltier heater/coolers could potentially replace standard compressors.[4] With the present efficiency of TE devices, such replacements are only reasonable when reliability and lifetime are more important than efficiency. The efficiency of a TE material is determined by the dimensionless figure of merit, $zT = \alpha^2\sigma\kappa^{-1}T$, where $T$ stands for temperature, $\alpha$ for Seebeck coefficient, $\sigma$ for electrical conductivity, and $\kappa$ for thermal conductivity. The numerator, $\alpha^2\sigma$, is commonly referred to as the power factor, and all of the thermoelectric parameters ($\alpha$, $\sigma$, and $\kappa$) are interdependent on each other and depend on the charge carrier concentration of the material.[2]

The CrN system is interesting for its hardness,[5,6] corrosion resistance,[7,8] near room-temperature magnetic phase transformation,[9−11] as well as TE properties.[12−16] Chromium is also a relatively cheap and abundant metal, allowing possible future mass production. The cubic NaCl B1 structure of $CrN_{1+\delta}$ (c-CrN) is of main interest with power factors in the range (1.5−5) $\times 10^{-3}$ W m$^{-1}$ K$^{-2}$ and a thermal conductivity around 4 W m$^{-1}$ K$^{-1}$, at room temperature.[15,17,18] Even though the material system appears relatively simple, the growth, control, and obtention of stoichiometric nitride coatings in physical vapor deposition (PVD) processes remain challenging. For instance, most PVD processes occur far from thermodynamic equilibrium. This allows synthesis of nitride films with large nitrogen composition variation maintaining the NaCl structure even if it would be thermodynamically metastable.[19−22] Controlling stoichiometry in CrN is essential to control its electrical and TE properties, because of the strong influence of the stoichiometry (nitrogen/vacancies) on charge carrier concentration in the CrN system. Nitrogen understoichiometry leads to increased n-type charge carriers, and nitrogen overstoichiometry yields p-type behavior of the coating.[13,23] For a deviation in stoichiometry larger than −0.3 in $CrN_{1+\delta}$, the hexagonal $Cr_2N$ (h-$Cr_2N$) secondary phase will typically appear.[13,21] This phase has metal-like electrical and thermoelectric properties. However, present as nanoinclusions in cubic CrN, it can be beneficial for the overall TE properties, since it injects charge carriers into the matrix phase without adversely affecting the overall Seebeck coefficient.[15,24]

Bulk powder nitride material can be synthesized by high-temperature annealing in ammonia ($NH_3$) atmosphere under thermodynamic equilibrium condition.[25] This process can also be used for post treatment as temperature annealing treatment for PVD films to increase the nitrogen content in the film and thus alter their properties.[10,18,26,27] In the Cr−N system, few reports have shown the effect of ammonia annealing on Cr−N films. Biswas et al. demonstrated a phase transformation from a mixture of h-$Cr_2N$/c-CrN to single-phase c-CrN upon

Received: June 10, 2024
Revised: July 17, 2024
Accepted: July 18, 2024
Published: July 30, 2024

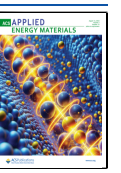

annealing in ammonia which yields metal-insulator behavior changes for its electrical transport.[10] Quintela et al. showed epitaxial CrN thin films becoming stoichiometric after annealing, with improved TE properties.[13,18] This emphasizes the need to investigate further and understand the effect of nitrogen stoichiometry and phase composition on the electrical and, more precisely, thermoelectric properties of CrN.

In the present work, we investigated the thermoelectric properties of $CrN_{1+\delta}$ films as-grown and annealed in ammonia. The initial as-grown coatings were either containing only NaCl-structured CrN or containing the NaCl-structured CrN with h-$Cr_2N$ secondary-phase inclusions. Those different films were annealed in $NH_3$ under different temperature conditions to mainly alter their nitrogen content, and the thermoelectric properties differences of the final film were investigated.

## EXPERIMENTAL SECTION

Two 59 nm films of NaCl-B1 structured CrN containing a secondary phase of h-$Cr_2N$ and two 52 nm single-phase (rock-salt cubic CrN) films were deposited on *c*-plane sapphire (10 × 10 × 0.5 $mm^3$ $Al_2O_3(0001)$) using unbalanced reactive direct current (DC) magnetron sputtering in an ultrahigh-vacuum chamber, described in detail elsewhere.[28] The Cr target (Kurt J. Lesker, 99.95%) had a diameter of 50.8 mm and a thickness of 6 mm. Throughout the deposition, the substrates were electrically floating with a constant substrate rotation of 15 rpm. A systematic waiting time of 15 min prior to deposition was implemented to allow temperature homogenization. All of the depositions lasted 30 min.

The deposition parameters of Cr−N were varied during an optimization process, leading to various phase constitutions in the films. The films with (without) secondary phase were deposited at a substrate temperature of 515 °C (570 °C), with a base pressure lower than $1.2 \times 10^{-5}$ Pa ($2.8 \times 10^{-7}$ Pa) and with a target power of 50 W (44 W). The films without secondary phase are denoted single phase (SP), and the films with a secondary phase are denoted mixed phase (MP). For the films labeled MP-1, the $Ar/N_2$ gas flows were 33/21 sccm, and the deposition pressure was 0.32 Pa. These parameters were 49/31 sccm and 0.47 Pa for the films labeled MP-2, and 22/33 sccm and 0.32 Pa for the single-phase films labeled SP-1 and SP-2, respectively.

The four deposited films were cut in half and annealed in a tubular furnace under a $NH_3$ flow. For each annealed temperature/duration, one MP film, one SP film, and one bare substrate, as reference, were reacted at 600 °C/2 h, 700 °C/2 h, 800 °C/2 h, and 800 °C/4 h. After the dwelling reaction time, the furnace was switched off and the nitride thin films were cooled down to room temperature under ammonia atmosphere. Before opening, the chamber was flushed with nitrogen.

The crystal structure of the samples was investigated by X-ray diffraction (XRD) using Bragg−Brentano mode ($\theta$–$2\theta$) with $\theta$ ranging from 15 to 90°. The equipment used was a PANalytical X'Pert Pro diffractometer, equipped with a Cu K$\alpha$ source operated at 45 kV and 40 mA. The incident optics was a Bragg−Brentano module with a 0.5° divergence slit and a 0.5° antiscatter slit, while the diffracted optics included a 5.0 mm antiscatter slit, a 0.04 rad Soller slit, a Ni-filter, and an X'Celerator detector. The thicknesses were determined by modeling X-ray reflectivity (XRR) measurements in the X'Pert Reflectivity software. Measurements were done using a PANalytical X'Pert diffractometer, equipped with a Cu K$\alpha$ source operated in line mode with a hybrid mirror module with a 0.5° divergence slit for incident optics and a 0.125° divergence slit for the diffracted optics. The same setup was used for rocking-curve measurements.

Scanning electron microscopy (SEM) imaging was performed in a Zeiss Sigma 300, with a field emission gun electron source. Top-view surface morphology images were acquired using a secondary electron detector with the electron gun operated at 2 kV.

The compositions of the films were determined by an ion-beam analysis technique, time-of-flight elastic recoil detection analysis (ToF-ERDA). Measurements were performed at Uppsala University.[29] ToF-ERDA measurements were performed using 36 MeV $^{127}I^{9+}$ ions as probing beam at a 67.5° incidence angle, relative to surface normal, and with the recoiled species detected at a 45° recoil angle. The data was analyzed using the Potku code.[30]

Room-temperature electrical sheet resistance was measured using a Jandell Model RM3000 4-point probe. The resistivities were measured after the samples were cut in half to ensure comparability before and after annealing. Two measurement points were taken along the cut and two across. The resistance of the films was then determined by multiplying the sheet resistance with the film thickness, to which a sample-size-dependent correction factor was applied. Typically an error bar of 5% (relative) is observed using this method.[31,32]

The Seebeck coefficient, $\alpha$, was measured at room temperature using a home-built thermoelectric measurement setup, equipped with two Peltier heat sources for creating a temperature gradient in the sample and two K-type thermocouples for measuring the temperature. The two Cu electrodes are in contact with the sample in an area of approximately 4 × 1 $mm^2$, in which thermocouples are present. The temperature gradient is applied in-plane over a distance of 8 mm. For all samples, the voltages were measured at five different $\Delta T$ (from 1 to 8 K) with a Keithley 2001 multimeter. Ag paste was applied on some of the samples to lower the contact resistance between the sample and Cu electrodes.

For the temperature-dependent in-plane Seebeck coefficient, the measurement was performed using ULVAC-RIKO ZEM3 under a low-pressure (0.9 atm) helium atmosphere from 100 °C up to 400 °C. For both Seebeck coefficient measurement setups, an error of 7% relative is observed.

## RESULTS

Figure 1 shows the $\theta$–$2\theta$ XRD patterns of the SP series and the MP series before and after annealing. The full-range XRD

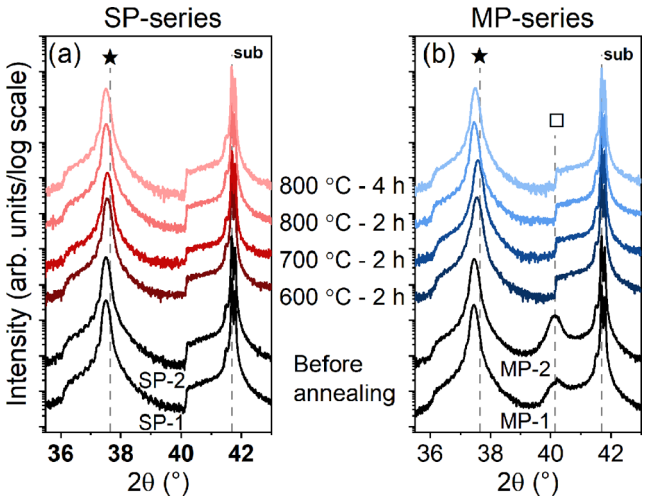


**Figure 1.** XRD $\theta/2\theta$ scans of as-grown and annealed films from the (a) SP series and (b) MP series. For both panels, the bottom two patterns are XRD scans from as-grown films. Marked reflections: star: cubic CrN 111; square: hexagonal $Cr_2N$ 0002; sub: $Al_2O_3$ 0006 from PDF 01-074-8390, 00-035-0803, and 00-046-1212, respectively.[33]

patterns are presented in the Supporting Information (Figure S1). The substrate 0006 peak is observed at 41.7° ($Al_2O_3(0006)$ reflection, PDF 00-046-1212).[33] A sharp increase originating from the Ni-filter cutoff of the substrate peak is seen around 40° for most of the diffractograms. Table 1 lists the *d* values and the corresponding rocking-curve full



https://doi.org/10.1021/acsaem.4c01491
ACS Appl. Energy Mater. 2024, 7, 6785−6792

Table 1. Measured $d_{111}$-Spacings (Growth Direction) and FWHM from $\omega$-Scan (Measured by Rocking Curve) of the As-Grown and Annealed Films from the SP and MP Series

| | | | As-grown | Annealed | |
|---|---|---|---|---|---|
| Series | Annealing conditions (temperature−duration) | Sample | $d_{111}$ ± 0.001 Å | $d_{111}$ ± 0.001 Å | $\omega$-FWHM ± 0.01° |
| SP | 600 °C−2 h | SP-1 | 2.397 | 2.394 | 0.05 |
| | 700 °C−2 h | SP-2 | 2.397 | 2.394 | 0.04 |
| | 800 °C−2 h | SP-1 | 2.397 | 2.397 | 0.05 |
| | 800 °C−4 h | SP-2 | 2.397 | 2.397 | 0.05 |
| MP | 600 °C−2 h | MP-1 | 2.401 | 2.394 | 0.05 |
| | 700 °C−2 h | MP-2 | 2.400 | 2.392 | 0.07 |
| | 800 °C−2 h | MP-1 | 2.401 | 2.400 | 0.05 |
| | 800 °C−4 h | MP-2 | 2.400 | 2.398 | 0.06 |

width at half-maximum (FWHM) for the two series of samples.

The XRD patterns from the as-deposited films show a peak at around 37.5°. This peak is identified as the (111) reflection from a cubic NaCl B1 structure (CrN, PDF 01-074-8390),[33] showing preferential growth along 111 for CrN. These films were part of the same deposition batches as in prior work where the epitaxial growth was demonstrated through pole figure analysis giving the following epitaxial relationship: $\langle 0001\rangle_s \| \langle 111\rangle_{film}$ (out of plane) and $(11\bar{2}0)_s \| (11\bar{2})_{film}$ or $(\bar{1}2\bar{1}0)_s \| (11\bar{2})_{film}$ (in-plane).[34] NaCl-structured materials are well known for their epitaxial growth with twin domains on *c*-plane sapphire.[35−39] For the MP series, an additional, broad peak is observed around 40.5°, identified as a (0002) reflection from hexagonal $Cr_2N$ (PDF 00-035-0803).[33] The presence of $Cr_2N$ can be observed in CrN films when the nitrogen content decreases, which has been reported in several works.[15,34]

After annealing, all diffraction patterns are similar to the presence of only the 111 XRD peak from CrN and a sharp Ni-filter cutoff at the substrate with no evidence of $Cr_2N$ phases. The absence of $Cr_2N$ is not directly concluded from the absence of the XRD peak as such, but rather by the well-defined Ni-filter cutoff at around 40.5° (Figure 1b) as seen for the SP series (Figure 1a). This reveals the efficacy of the annealing process for eliminating the secondary phase. The measured $d_{111}$-spacings of CrN after annealing correspond to lattice parameter $a$ = 4.14−4.16 Å, in agreement with previous work and theoretical values of 4.13 Å.[10,13,34,40] For the SP series, the CrN 111 peak of the films annealed at 600 and 700 °C shifted by +0.04−0.05° toward higher angles. On the other hand, after annealing at 800 °C, the diffraction peaks shifted back to a lower angle and happened to be at the same position as the as-grown film. In the MP series, similar variations are observed with a shift of the 111 diffraction peak of CrN toward a higher angle of +0.1° when annealed at 600 or 700 °C. Similar to the SP series, the 111 diffraction peak of the MP series films annealed at 800 °C shifted back to lower angles and at a position close to the as-grown peak position. All of the different values of the $d_{111}$ spacing are listed in Table 1.

XRD analysis reveals that any secondary phases previously observed have been removed after annealing regardless of the temperature and duration of annealing. Annealing in ammonia affects the $d_{111}$ spacing of the CrN materials and could be related to composition variation and strain relaxation. With a mismatch of approximately +11% with *c*-plane sapphire,[38] the as-grown CrN film grown epitaxially on sapphire may suffer compressive strain, hence an observation of larger out-of-plane $d_{111}$ than its relaxed position. Strain relaxation of compressive films would lead to an XRD peak shift to a higher angle than observed as, for example, the as-grown film (Figure 1).

The quality of the orientation of the film after annealing was evaluated with the rocking-curve measurement performed on the 111-reflection from CrN at $2\theta$ = 37.5° (Table 1). The rocking curve of the annealed SP films has a $\omega$-FWHM of 0.05° or lower. The MP-1 films showed an FWHM of 0.05°, while the MP-2 films demonstrated a larger value of 0.05−0.07°. No clear trends are observed on the effect of annealing temperature or duration on the quality of the preferential orientation. Nevertheless, a larger FWHM of 0.07° was observed for the films (MP-2) initially containing a relatively larger amount of $Cr_2N$ prior to deposition (Table 1). For all annealed films, the $\omega$-FWHM of the CrN 111 peaks remain relatively low between 0.04 and 0.07°.

Table 2 lists the ToF-ERDA compositions of the films from the two series of samples after annealing at different conditions. For clarity, the compositions were written as $Cr_1N_{1+\delta}$ and $Cr_1(O,N)_{1+\gamma}$ to compare the series and evaluate their stoichiometry variations. With the exception of the 800−2 h sample which has $\delta$ = +0.08, the difference of N content in the SP series varies between $\delta$ = −0.05 and −0.02. The deviation from stoichiometry is relatively larger for the annealed MP series with values of $\delta$ between −0.09 and −0.06. Apart from SP 800−2 h, the annealed SP samples are on average closer to stoichiometry with $\delta \approx -0.04$, compared to the annealed MP series with $\delta \approx -0.08$.

Table 2. Composition Analysis of the Two Series (SP and MP) Annealed under Different Temperatures and Times[a]

| | | | Composition, ToF-ERDA, $\delta$ and $\gamma$ with ±0.02 | |
|---|---|---|---|---|
| Series | Annealing conditions (temperature−duration) | Sample | $CrN_{1+\delta}$ | $Cr(N,O)_{1+\gamma}$ |
| SP | 600 °C−2 h | SP-1 | $CrN_{0.98}$ | $Cr(N,O)_{1.01}$ |
| | 700 °C−2 h | SP-2 | $CrN_{0.95}$ | $Cr(N,O)_{0.97}$ |
| | 800 °C−2 h | SP-1 | $CrN_{1.08}$ | $Cr(N,O)_{1.13}$ |
| | 800 °C−4 h | SP-2 | $CrN_{0.96}$ | $Cr(N,O)_{1.00}$ |
| MP | 600 °C−2 h | MP-1 | $CrN_{0.93}$ | $Cr(N,O)_{0.95}$ |
| | 700 °C−2 h | MP-2 | $CrN_{0.92}$ | $Cr(N,O)_{0.95}$ |
| | 800 °C−2 h | MP-1 | $CrN_{0.94}$ | $Cr(N,O)_{0.97}$ |
| | 800 °C−4 h | MP-2 | $CrN_{0.91}$ | $Cr(N,O)_{0.94}$ |

[a]The composition is after annealing.

Oxygen contamination was detected for all films with approximately 1−2 at. %, which corresponds to the lower detection limit of ToF-ERDA. When considering an insertion



https://doi.org/10.1021/acsaem.4c01491
ACS Appl. Energy Mater. 2024, 7, 6785−6792

of oxygen in the NaCl structure as in $Cr_1(N,O)_{1+\gamma}$, the deviation to stoichiometry in the NaCl B1 structure is further reduced with $\gamma \approx 0$ for the SP series and $\gamma \approx -0.05$ for the MP series. For reference, a deviation to stoichiometry of $\delta = -0.08$ with oxygen levels below 2 at. % was measured on films with nominally identical deposition conditions as for the SP films.[34] The composition of the MP series was not quantified before annealing. Although these films had two phases, h-$Cr_2N$ and c-CrN, this reveals that the nitrogen content is significantly lower than in the SP series. For comparison with other work, an epitaxial c-CrN on *c*-plane sapphire had a deviation to stoichiometry of $\delta \approx -0.15$ while maintaining single-phase NaCl CrN structure.[15,41]

An increase of N in the NaCl structure from an understoichiometric $CrN_{1+\delta}$ with $\delta < 0$ would lead to an increase of the cell parameters, hence a shift of the XRD peak towards lower angles. No clear trends and conclusions could be drawn from XRD as two phenomena have an effect on the position of the XRD peak. The compressive stress yields a shift toward smaller angles and its relaxation to a shift toward larger angles, while the insertion of N in the NaCl structure yields a shift toward lower angles.

Figure 2 shows the room-temperature thermoelectric properties with the electrical resistivity ($\rho$), the Seebeck coefficient ($\alpha$), and the power factor ($\alpha^2\sigma = \alpha^2\rho^{-1}$) of the as-grown films and annealed. Before annealing, the SP samples exhibited resistivity values around 40−50 mΩ cm and Seebeck coefficient values of around −40 to −50 $\mu$V K$^{-1}$, leading to a power factor between 3 and 5 $\mu$W m$^{-1}$ K$^{-2}$. The variation of electrical and thermoelectric properties between the samples (prior to annealing) could be due to a small variation of stoichiometry or morphology that can occur between deposition batches. The variation remained low and should not be seen as an anomaly. After annealing, regardless of the annealing conditions, the electrical resistivity drastically increased to values between 420 and 770 mΩ cm, and the measured Seebeck coefficient values decreased by a factor of 2 compared to the as-grown films. The calculated power factor for the annealed film is reduced to values close to 0.1 $\mu$W m$^{-1}$ K$^{-2}$.

The as-grown film from the MP series, i.e., containing $Cr_2N$ as secondary phase, exhibited electrical resistivity values around 6−7 mΩ cm and Seebeck coefficient values near −57 $\mu$V K$^{-1}$. This resulted in a power factor of around 50 $\mu$W m$^{-1}$ K$^{-2}$. After annealing, the electrical resistivity remained relatively the same with a small reduction from 6−7 to 3.5 mΩ cm for the annealed MP film at 800 °C. However, the room-temperature absolute Seebeck coefficient values increased to values larger than 100 $\mu$V K$^{-1}$ for the films annealed at 600 and 700 °C and to a maximum of 130 $\mu$V K$^{-1}$ when annealed at 800 °C for 2 h. A longer annealing time at 800 °C yielded a reduction in the absolute Seebeck coefficient values to −82 $\mu$V K$^{-1}$. Both electrical resistivity and Seebeck coefficient for the MP series improved after ammonia annealing. The resulting power factor of the samples annealed in the MP series increased from around 50 to 130−480 $\mu$W m$^{-1}$ K$^{-2}$, with the most pronounced increase for an annealing at 800 °C for 2 h.

Previous reports showed a large variation of the electrical and thermoelectric properties of CrN films. Typical values of resistivity can range from 1 to 60 mΩ cm and the Seebeck coefficient can range from 25 to 400 $\mu$V K$^{-1}$.[14−18] In the present manuscript, only the annealed MP films are on par

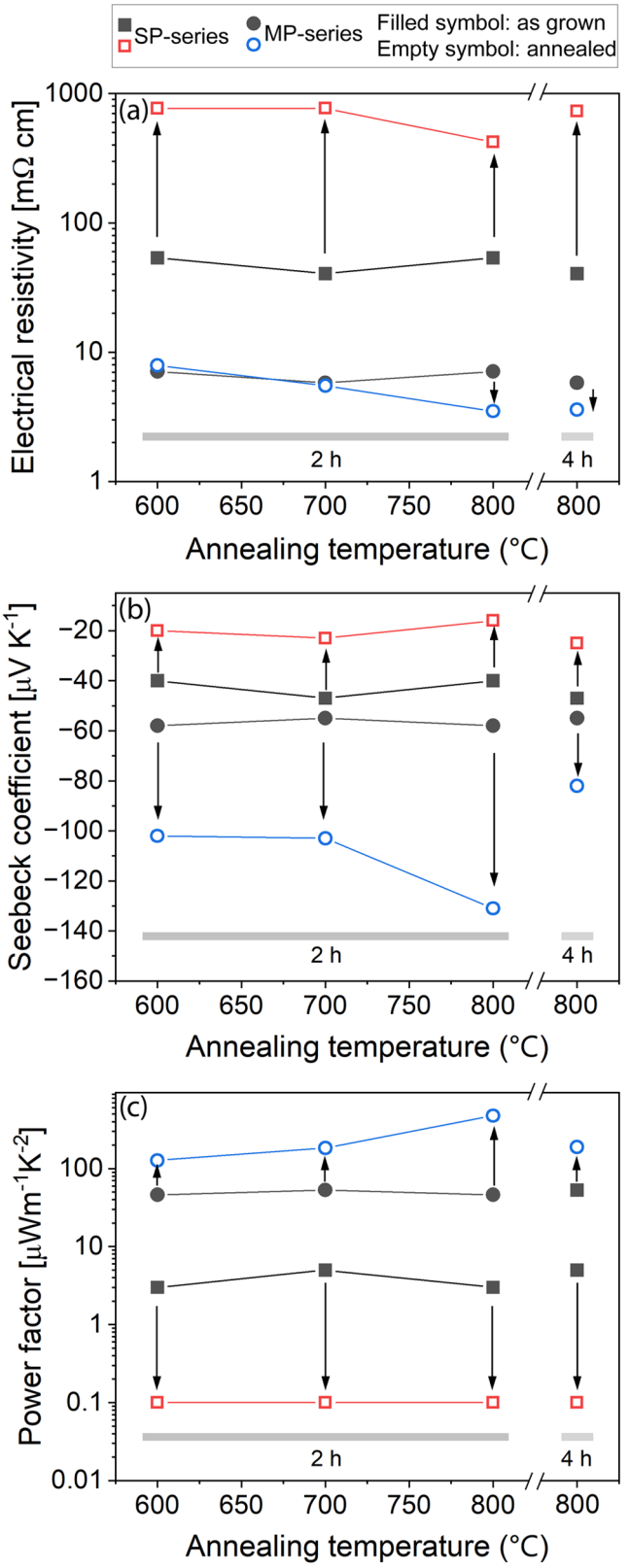


**Figure 2.** Room-temperature thermoelectric properties: (a) electrical resistivity, (b) Seebeck coefficient, and (c) power factor for all samples: before (filled symbol) and after (empty symbol) ammonia annealing performed at different temperatures and durations. The arrows show the changes occurring after annealing.



https://doi.org/10.1021/acsaem.4c01491
ACS Appl. Energy Mater. 2024, 7, 6785−6792

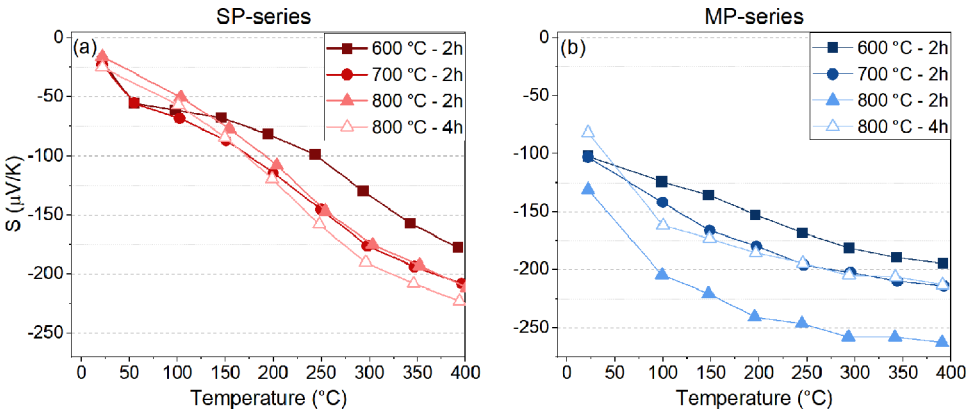


**Figure 3.** Seebeck coefficient as a function of temperature. Values at elevated temperatures (above room temperature) are measured by ZEM3, while the values at 22 °C are measured in the home-built thermoelectric measurement setup. (a) SP series and (b) MP series.

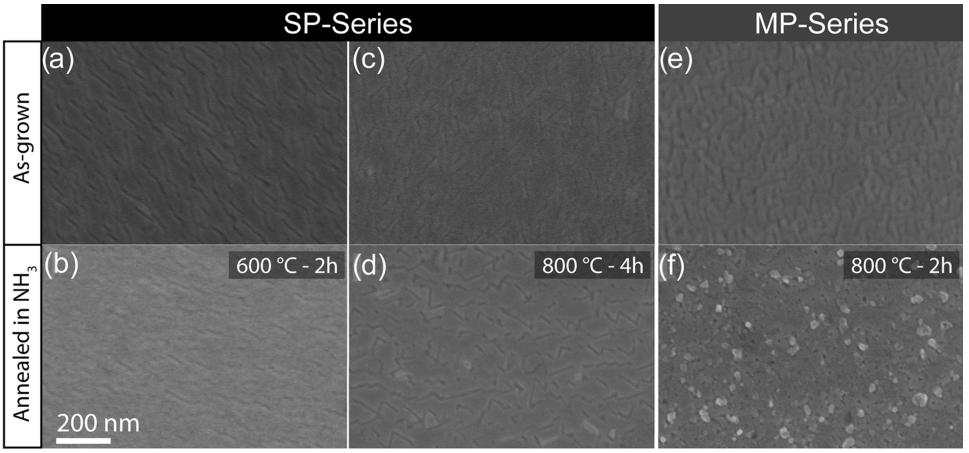


**Figure 4.** SEM surface morphology images of select films, as-grown (a, c, e) and after annealing (b, d, f). As denoted, pairs (a, b), (c, d), and (e, f) are the samples SP 600−2 h, SP 800−4 h, and MP 800−2 h, respectively.

with the reported values, and the annealed SP series have orders of magnitude larger resistivity and much lower Seebeck coefficient values at room temperature.

Figure 3 shows the temperature-dependent Seebeck coefficient values measured by ZEM3 of the annealed samples. The room-temperature values reported in the graph are the values measured with the home-built thermoelectric measurement setup presented in Figure 2. Note that only Seebeck coefficient values are shown. The Seebeck coefficient measurements were repeated twice showing equivalent results with no changes occurring during the measurement revealing stability in the temperature of the film in the measurement range. Moreover, these measurements are consistent with the result obtained at room temperature by other measurement techniques and previous results already reported for these kinds of compound.[14−18]

All films, from SP and MP series, exhibited similar trends of the Seebeck coefficient with temperature. An increase in the Seebeck coefficient values is observed monotonically from room temperature up to the maximum measurement temperature. In the SP series, the annealed 600−2 h film differs from the rest of this series, with slightly lower absolute Seebeck coefficient values above 200 °C (Figure 3a). All three other annealed films exhibited similar trends, with the Seebeck coefficient varying from −50 $\mu$V K$^{-1}$ at 100 °C to −220 $\mu$V K$^{-1}$ at 400 °C. All annealed MP series (Figure 3b) exhibited similar temperature-dependent Seebeck coefficient values but with larger absolute values at lower temperatures than the SP series. The 600−2 h annealed MP sample exhibits relatively lower values throughout the temperature range. An increase of temperature leads to an overall increase of the Seebeck coefficient in the entire range of measurement temperature. The annealed MP 800−2 h sample exhibited a significantly larger Seebeck coefficient value, with maximum absolute values above 200 $\mu$V K$^{-1}$ in the temperature range 100−400 °C and a maximum measured value of 250 above 250 °C. A longer duration of annealing at 800 °C led to a decrease in the Seebeck coefficient values. The thermoelectric properties of Cr−N films can be compared to the power factor of other thermoelectric thin-film materials at room temperature, like n-type $Bi_2T_3$ (4000 $\mu$W m$^{-1}$ K$^{-2}$),[42] n-type PbTe (1500 $\mu$W m$^{-1}$ K$^{-2}$),[43] and p-type $Ca_3Co_4O_9$ (800 $\mu$W m$^{-1}$ K$^{-2}$).[44]

Figure 4 displays the SEM images of selected samples. The top row (a, c, e) presents the images of as-grown film surfaces, and the bottom row (b, d, f) shows the surface images of the corresponding annealed films. Figure 4a−d corresponds to the SP series films 600−2 h and 800−4 h which were the extreme end annealing conditions tested in this study. Regardless of the phase composition, the as-grown films (Figure 4a−c) have large, elongated grains (≈50 × 300−1000 nm). After annealing, this morphology feature was retained for the film containing originally single-phase CrN (Figure 4b,d), with the observation of enlarged grains for both of these samples which is more pronounced for higher annealing temperature. The



https://doi.org/10.1021/acsaem.4c01491
ACS Appl. Energy Mater. 2024, 7, 6785−6792

films with originally a mix of CrN and $Cr_2N$ (Figure 4e,f) undergo a change of morphology from a relatively smooth film with elongated grains (Figure 4e) to a rougher film without elongated grains and the presence of visible voids (Figure 4f).

The as-grown SP films exhibited lower absolute Seebeck coefficient and higher electrical resistivity than previously reported values for pure cubic CrN thin films ($\alpha$: −100 to −240 $\mu$V $K^{-1}$, $\rho$: 0.75−15 mΩ cm).[15,17,18,34] Several factors play an important role in the electrical and thermoelectric properties of CrN, where nitrogen vacancies, oxygen contamination, and morphology are the most important aspects.[13,45]

In the present study, from the composition analysis (Table 2) and diffractograms (Figure 1), we observed that annealing in ammonia increased the nitrogen content in the films as well as transformed the multiphases h-$Cr_2N$/c-CrN phase into a single-phase c-CrN film. This annealing effect was expected and is in line with the rest of the literature.[10] After annealing, the morphology in the SP series was unchanged, and the composition analysis revealed a change of deviation from stoichiometry in $CrN_{1+\delta}$ from $\delta$ = −0.08 to $\delta$ = −0.05 to −0.02. This confirmed that nitrogen has been incorporated in the films upon annealing, whereas no trends have been observed for different temperatures.

In the SP series, after annealing, the vacancies ($\delta$) were reduced to a level of $\delta$ = −0.02/−0.04 as in $CrN_{1+\delta}$, or $\gamma \approx 0$ as in $Cr(N,O)_{1+\gamma}$ when considering oxygen as doping element in the NaCl structure. Those variations resulted in a reduction of the Seebeck coefficient as well as an increase of the electrical resistivity in the range of insulators, which are not anymore typical values for a degenerated semiconductor.

The MP series films, on the other hand, experienced several changes upon annealing, yielding substantial improvements of their TE properties. The phase composition changed from mix-phase to single-phase-containing films, the nitrogen content varied, and the surface morphology changed. In this film series, the deviation to stoichiometry as in $CrN_{1+\delta}$ became $\delta$ = −0.08 after annealing. Compositional analysis showed that they still have a significant understoichiometry even considering that oxygen is inserted into the NaCl structure: $Cr(N,O)_{1+\gamma}$ with $\gamma$ = −0.05. The reduction of electrical resistivity observed for the film annealed at 800 °C seems to be related more to a lower level of electron scattering since the composition of the films is relatively the same in this series. Indeed, the annealing at higher temperatures may have affected the grain boundaries and/or morphology of the film, hence affecting the electron scattering.

In CrN, the presence of vacancies and or oxygen contamination plays an important role and influences the charge carrier concentration.[13] A non-negligible amount of oxygen content was detected in the films, which will affect the charge carrier concentration, hence the Seebeck coefficient. A previous work has shown that a gradual variation of the nitrogen content in the CrN structure yields an n-type to p-type semiconductor behavior with a reduction to nominally a zero value for the Seebeck coefficient at the transition which happens for a film close to stoichiometry ($\delta \approx 0$).[13]

Upon ammonia annealing, the samples initially having a mixture of c-CrN and h-$Cr_2N$ (MP series) had their Seebeck coefficient increased and their electrical resistivity remaining at the same scale or slightly decreased for higher temperatures. On the other hand, samples initially composed of a single phase of CrN (SP series) had their Seebeck coefficient decreased, and their electrical resistivity increased. The composition of the film (Table 2) revealed that the annealed MP samples have a larger nitrogen understoichiometry ($\delta \approx$ −0.07), compared to the annealed SP samples ($\delta \approx$ −0.04). Biswas et al. have previously shown that a mix-phase c-CrN/h-$Cr_2N$ film undergoes to phase transition to single-phase c-CrN when annealed, yielding a large increase of electrical resistivity.[10] Other studies showed improvement of TE properties (resistivity and Seebeck values) upon annealing of a single-phase c-CrN film which is different from our findings.[18] Quintela et al. reported the annealing study of highly understoichiometric single-phase $CrN_{1+\delta}$ film with $\delta$ = −0.25.[18] After ammonia annealing, they claimed the obtention of a stoichiometric CrN (composition measured by electron energy loss spectroscopy, EELS), but no composition values were reported. More recent studies reported the importance of a small deviation to stoichiometry, where $\delta \approx$ −0.07 will give a significant difference in the thermoelectric properties of $CrN_{1+\delta}$.[13] The TE properties of the films are highly dependent on stoichiometry, where ammonia annealing plays a role in reducing the deviation to stoichiometry. Its effect seems to be dependent on the initial level of deviation to stoichiometry. In fact, it is possible that the work reported by Quintela et al. reported an increase of the TE properties of CrN after annealing by obtaining a nearly stoichiometric CrN with a few nitrogen vacancies not necessarily detectable by EELS. With this small deviation from stoichiometry, those results are in line with our findings. When the nitrogen vacancies are reduced in $CrN_{1+\delta}$ but not entirely removed, an improvement of the TE properties is observed before observing a deterioration of its TE properties when the stoichiometry is achieved.

Quintela et al. demonstrated that ammonia annealing of CrN can greatly improve its TE properties.[18] We have demonstrated that ammonia annealing of the CrN system will not systematically improve its TE properties. The effect of ammonia annealing is highly dependent on the composition beforehand and its deviation to stoichiometry. In contradiction with this, the Seebeck coefficient values at elevated temperatures did not differ much between our two series. In line with the work of Biswas et al., we also saw that such a secondary phase is eliminated upon annealing in ammonia.[10] Phase control and stoichiometry tailoring can be achieved during the deposition process by magnetron sputtering, but remain rather challenging. Temperature, pressure, nitrogen flow, and target power density are a few parameters that have an impact on phase and stoichiometry. Substrate selection is of significant importance where c-CrN is favored on MgO(100) even with a large deviation to stoichiometry ($\delta > -0.25$)[13] while growing on $Al_2O_3$(0001) h-$Cr_2N$ is favored for a smaller deviation of stoichiometry in $CrN_{1+\delta}$ ($\delta > -0.15$).[13,15,41] With challenging control of the stoichiometry during sputtering growth, annealing in ammonia seems to be an effective way of controlling the stoichiometry along with the phase formation in the film. However, the resulting film stoichiometry and properties are dependent on the stoichiometry before annealing treatment. The present study highlights the importance of individual ammonolysis condition optimization dependent on the initial stoichiometry of the film. In the present work, annealing at 800 °C/2 h yields great improvements in the TE properties on a mix-phase-containing film while being detrimental when performed on a single-phase film with relatively lower deviation to stoichiometry.



https://doi.org/10.1021/acsaem.4c01491
ACS Appl. Energy Mater. 2024, 7, 6785−6792

## CONCLUSIONS

The effect of high-temperature ammonia annealing of Cr−N films on their thermoelectric properties was investigated. Ammonia annealing of mix-phase cubic CrN/hexagonal-Cr2N leads to single-phase cubic CrN with a greatly improved power factor ($(0.1-0.5) \times 10^{-3}$ W m$^{-1}$ K$^{-2}$) compared to the as-grown films ($0.05 \times 10^{-3}$ W m$^{-1}$ K$^{-2}$). In contrast, the single-phase cubic CrN films undergoing the same annealing conditions see their thermoelectric properties deteriorate after annealing (power factor from $4 \times 10^{-6}$ to less than $1 \times 10^{-7}$ W m$^{-1}$ K$^{-2}$), mainly due to larger electrical resistivities. Those observations underscore the importance of controlling the nitrogen vacancies in the CrN system to maximize its thermoelectric material. Ammonia annealing of Cr−N coatings does not necessarily lead to an improvement in thermoelectric properties. Nevertheless, under optimized conditions and depending on the deviation to stoichiometry prior to annealing as in $CrN_{1+\delta}$, the thermoelectric properties can be greatly improved. Employing postdeposition ammonia annealing could be used instead of meticulous deposition control to grow high-performing films of CrN for thermoelectric applications.

## ASSOCIATED CONTENT

### Supporting Information

The Supporting Information is available free of charge at https://pubs.acs.org/doi/10.1021/acsaem.4c01491.

Full-range XRD pattern of the as-grown and annealed samples from the two samples series and their descriptions (PDF)

## AUTHOR INFORMATION


### Corresponding Author

**Victor Hjort** − *Thin Film Physics Division, Department of Physics, Chemistry, and Biology (IFM), Linköping University, SE-581 83 Linköping, Sweden;* orcid.org/0009-0006-4871-8734; Email: victor.hjort@liu.se

### Authors

**Franck Tessier** − *Univ. Rennes, CNRS, ISCR (Institut des Sciences Chimiques de Rennes)—UMR 6226, F-35000 Rennes, France;* orcid.org/0000-0002-1253-7011

**Fabien Giovannelli** − *GREMAN UMR 7347, Université de Tours, CNRS, INSA CVL, IUT de Blois, F-41029 Blois, France;* orcid.org/0000-0003-1248-077X

**Arnaud le Febvrier** − *Thin Film Physics Division, Department of Physics, Chemistry, and Biology (IFM), Linköping University, SE-581 83 Linköping, Sweden;* orcid.org/0000-0002-3059-7392

**Per Eklund** − *Thin Film Physics Division, Department of Physics, Chemistry, and Biology (IFM), Linköping University, SE-581 83 Linköping, Sweden; Inorganic Chemistry, Department of Chemistry—Ångström Laboratory, Uppsala University, SE-751 21 Uppsala, Sweden;* orcid.org/0000-0003-1785-0864

Complete contact information is available at: https://pubs.acs.org/10.1021/acsaem.4c01491


### Notes

The authors declare no competing financial interest.

## ACKNOWLEDGMENTS

The authors acknowledge funding from the Swedish Government Strategic Research Area in Materials Science on Functional Materials at Linköping University (Faculty Grant SFO-Mat-LiU No. 2009 00971), the Knut and Alice Wallenberg Foundation through the Wallenberg Academy Fellows program (KAW-2020.0196), the Swedish Research Council (VR) under Project No. 2021-03826, and the Swedish Energy Agency under project number 52740-1. Daniel Primetzhofer from Uppsala University is acknowledged for ion-beam measurements. Sanath Kumar Honnali from Linköping University is acknowledged for input on the analysis of ToF-ERDA data. Accelerator operation is supported by Swedish Research Council VR-RFI (Contract No. 2019-00191) and the Swedish Foundation for Strategic Research (Contract No. RIF14-0053).

## REFERENCES


(1) Shi, X.-L.; Zou, J.; Chen, Z.-G. Advanced Thermoelectric Design: From Materials and Structures to Devices. *Chem. Rev.* **2020**, *120* (15), 7399−7515.

(2) Snyder, G. J.; Toberer, E. S. Complex Thermoelectric Materials. *Nat. Mater.* **2008**, *7* (2), 105−114.

(3) Mao, J.; Liu, Z.; Zhou, J.; Zhu, H.; Zhang, Q.; Chen, G.; Ren, Z. Advances in Thermoelectrics. *Adv. Phys.* **2018**, *67* (2), 69−147.

(4) DiSalvo, F. J. Thermoelectric Cooling and Power Generation. *Science* **1999**, *285* (5428), 703−706.

(5) Berg, G.; Friedrich, C.; Broszeit, E.; Berger, C. Development of Chromium Nitride Coatings Substituting Titanium Nitride. *Surf. Coat. Technol.* **1996**, *86*−*87*, 184−191.

(6) Kabir, M. S.; Munroe, P.; Zhou, Z.; Xie, Z. Structure and Mechanical Properties of Graded Cr/CrN/CrTiN Coatings Synthesized by Close Field Unbalanced Magnetron Sputtering. *Surf. Coat. Technol.* **2017**, *309*, 779.

(7) Liu, C.; Bi, Q.; Matthews, A. EIS Comparison on Corrosion Performance of PVD TiN and CrN Coated Mild Steel in 0.5 N NaCl Aqueous Solution. *Corros. Sci.* **2001**, *43* (10), 1953−1961.

(8) Subramanian, B.; Jayachandran, M. Preparation of Chromium Oxynitride and Chromium Nitride Films by DC Reactive Magnetron Sputtering and Their Material Properties. *Corros. Eng., Sci. Technol.* **2011**, *46* (4), 554−561.

(9) Filippetti, A.; Hill, N. A. Magnetic Stress as a Driving Force of Structural Distortions: The Case of CrN. *Phys. Rev. Lett.* **2000**, *85* (24), 5166−5169.

(10) Biswas, B.; Chakraborty, S.; Joseph, A.; Acharya, S.; Pillai, A. I. K.; Narayana, C.; Bhatia, V.; Garbrecht, M.; Saha, B. Secondary Phase Limited Metal-Insulator Phase Transition in Chromium Nitride Thin Films. *Acta Mater.* **2022**, *227*, No. 117737.

(11) Biswas, B.; Rudra, S.; Rawat, R. S.; Pandey, N.; Acharya, S.; Joseph, A.; Pillai, A. I. K.; Bansal, M.; de h-Óra, M.; Panda, D. P.; Dey, A. B.; Bertram, F.; Narayana, C.; MacManus-Driscoll, J.; Maity, T.; Garbrecht, M.; Saha, B. Magnetic Stress-Driven Metal-Insulator Transition in Strongly Correlated Antiferromagnetic CrN. *Phys. Rev. Lett.* **2023**, *131* (12), No. 126302.

(12) Eklund, P.; Kerdsongpanya, S.; Alling, B. Transition-Metal-Nitride-Based Thin Films as Novel Energy Harvesting Materials. *J. Mater. Chem. C* **2016**, *4* (18), 3905−3914.

(13) le Febvrier, A.; Gambino, D.; Giovannelli, F.; Bakhit, B.; Hurand, S.; Abadias, G.; Alling, B.; Eklund, P. P-Type Behavior of CrN Thin Films via Control of Point Defects. *Phys. Rev. B* **2022**, *105* (10), No. 104108.

(14) Gharavi, M. A.; Gambino, D.; le Febvrier, A.; Eriksson, F.; Armiento, R.; Alling, B.; Eklund, P. High Thermoelectric Power Factor of Pure and Vanadium-Alloyed Chromium Nitride Thin Films. *Mater. Today Commun.* **2021**, *28*, No. 102493.

(15) Gharavi, M. A.; Kerdsongpanya, S.; Schmidt, S.; Eriksson, F.; Nong, N. V.; Lu, J.; Balke, B.; Fournier, D.; Belliard, L.; le Febvrier,

A.; Pallier, C.; Eklund, P. Microstructure and Thermoelectric Properties of CrN and CrN/Cr2N Thin Films. *J. Phys. D: Appl. Phys.* **2018**, *51* (35), No. 355302.
(16) Quintela, C. X.; Rivadulla, F.; Rivas, J. Thermoelectric Properties of Stoichiometric and Hole-Doped CrN. *Appl. Phys. Lett.* **2009**, *94* (15), No. 152103.
(17) Jankovský, O.; Sedmidubský, D.; Huber, Š.; Šimek, P.; Sofer, Z. Synthesis, Magnetic and Transport Properties of Oxygen-Free CrN Ceramics. *J. Eur. Ceram. Soc.* **2014**, *34* (16), 4131−4136.
(18) Quintela, C. X.; Podkaminer, J. P.; Luckyanova, M. N.; Paudel, T. R.; Thies, E. L.; Hillsberry, D. A.; Tenne, D. A.; Tsymbal, E. Y.; Chen, G.; Eom, C.-B.; Rivadulla, F. Epitaxial CrN Thin Films with High Thermoelectric Figure of Merit. *Adv. Mater.* **2015**, *27* (19), 3032−3037.
(19) Kang, J. H.; Kim, K. J. Structural, Optical, and Electronic Properties of Cubic TiNx Compounds. *J. Appl. Phys.* **1999**, *86* (1), 346−350.
(20) Subramanian, B.; Prabakaran, K.; Jayachandran, M. Influence of Nitrogen Flow Rates on Materials Properties of CrNxfilms Grown by Reactive Magnetron Sputtering. *Bull. Mater. Sci.* **2012**, *35* (4), 505−511.
(21) Hones, P.; Martin, N.; Regula, M.; Lévy, F. Structural and Mechanical Properties of Chromium Nitride, Molybdenum Nitride, and Tungsten Nitride Thin Films. *J. Phys. D: Appl. Phys.* **2003**, *36* (8), 1023.
(22) Rutberg, V. Synthesis and Thermoelectric Properties of Cr1-xMexN (Me = Mo, V), 2022. Retrieved from https://urn.kb.se/resolve?urn=urn:nbn:se:liu:diva-188198.
(23) Mozafari, E.; Alling, B.; Steneteg, P.; Abrikosov, I. A. Role of N Defects in Paramagnetic CrN at Finite Temperatures from First Principles. *Phys. Rev. B* **2015**, *91* (9), No. 094101.
(24) Biswas, B.; Chakraborty, S.; Chowdhury, O.; Rao, D.; Pillai, A. I. K.; Bhatia, V.; Garbrecht, M.; Feser, J. P.; Saha, B. In-Plane Cr 2 N − CrN Metal-Semiconductor Heterostructure with Improved Thermoelectric Properties. *Phys. Rev. Mater.* **2021**, *5* (11), No. 114605.
(25) Johnson, W. C.; Parson, J. B.; Crew, M. C. Nitrogen Compounds of Gallium. III. *J. Phys. Chem. A* **1932**, *36* (10), 2651−2654.
(26) Zhuravlev, K.; Malin, T.; Mansurov, V.; Novikova, N.; Yakovlev, V. Effect of Annealing and Nitridation on (0001) Sapphire Surface Polaritons. *Phys. Status Solidi C* **2013**, *10* (3), 377−380.
(27) Malin, T.; Mansurov, V.; Galitsyn, Y.; Zhuravlev, K. Thermodynamic and Kinetic Aspects of AlN Crystal Formation on (0001)$Al_2O_3$ Surface by Ammonia MBE. *Phys. Status Solidi C* **2014**, *11* (3−4), 613−616.
(28) le Febvrier, A.; Landälv, L.; Liersch, T.; Sandmark, D.; Sandström, P.; Eklund, P. An Upgraded Ultra-High Vacuum Magnetron-Sputtering System for High-Versatility and Software-Controlled Deposition. *Vacuum* **2021**, *187*, No. 110137.
(29) Mayer, M.; Möller, S.; Rubel, M.; Widdowson, A.; Charisopoulos, S.; Ahlgren, T.; Alves, E.; Apostolopoulos, G.; Barradas, N. P.; Donnelly, S.; Fazinić, S.; Heinola, K.; Kakuee, O.; Khodja, H.; Kimura, A.; Lagoyannis, A.; Li, M.; Markelj, S.; Mudrinic, M.; Petersson, P.; Portnykh, I.; Primetzhofer, D.; Reichart, P.; Ridikas, D.; Silva, T.; Gonzalez de Vicente, S. M.; Wang, Y. Q. Ion Beam Analysis of Fusion Plasma-Facing Materials and Components: Facilities and Research Challenges. *Nucl. Fusion* **2019**, *60* (2), No. 025001.
(30) Arstila, K.; Julin, J.; Laitinen, M. I.; Aalto, J.; Konu, T.; Kärkkäinen, S.; Rahkonen, S.; Raunio, M.; Itkonen, J.; Santanen, J.-P.; Tuovinen, T.; Sajavaara, T. Potku − New Analysis Software for Heavy Ion Elastic Recoil Detection Analysis. *Nucl. Instrum. Methods Phys. Res., Sect. B* **2014**, *331*, 34−41.
(31) Topsoe, H. *Geometric Factors in Four Point Resistivity Measurement*, 1968. No. 2nd revised edition.
(32) Miccoli, I.; Edler, F.; Pfnür, H.; Tegenkamp, C. The 100th Anniversary of the Four-Point Probe Technique: The Role of Probe Geometries in Isotropic and Anisotropic Systems. *J. Phys.: Condens. Matter* **2015**, *27* (22), No. 223201.
(33) Gates-Rector, S.; Blanton, T. The Powder Diffraction File: A Quality Materials Characterization Database. *Powder Diffr.* **2019**, *34* (4), 352−360.
(34) Hjort, V.; Singh, N. K.; Chowdhury, S.; Shu, R.; Le Febvrier, A.; Eklund, P. Phase Composition and Thermoelectric Properties of Epitaxial CrMoVN Thin Films. *Adv. Energy Sustainability Res.* **2023**, *4* (12), No. 2300119.
(35) Dai, Z. N.; Miyashita, A.; Yamamoto, S.; Narumi, K.; Naramoto, H. Crystalline and Nearly Stoichiometric Vanadium Nitride Thin Film by PLD. *Thin Solid Films* **1999**, *347* (1), 117−120.
(36) Stampe, P. A.; Bullock, M.; Tucker, W. P.; Kennedy, R. J. Growth of MgO Thin Films on M-, A-, C- and R-Plane Sapphire by Laser Ablation. *J. Phys. D: Appl. Phys.* **1999**, *32* (15), 1778.
(37) Li, R.; Gandhi, J. S.; Pillai, R.; Forrest, R.; Starikov, D.; Bensaoula, A. Epitaxial Growth of (111)-Oriented ZrxTi1−xN Thin Films on c-Plane Al2O3 Substrates. *J. Cryst. Growth* **2014**, *404*, 1−8.
(38) Le Febvrier, A.; Tureson, N.; Stilkerich, N.; Greczynski, G.; Eklund, P. Effect of Impurities on Morphology, Growth Mode, and Thermoelectric Properties of (1 1 1) and (0 0 1) Epitaxial-like ScN Films. *J. Phys. D: Appl. Phys.* **2019**, *52* (3), No. 035302.
(39) Jin, Q.; Wang, Z.; Zhang, Q.; Zhao, J.; Cheng, H.; Lin, S.; Chen, S.; Chen, S.; Guo, H.; He, M.; Ge, C.; Wang, C.; Wang, J.-O.; Gu, L.; Wang, S.; Yang, H.; Jin, K.; Guo, E.-J. Structural Twinning-Induced Insulating Phase in CrN (111) Films. *Phys. Rev. Mater.* **2021**, *5* (2), No. 023604.
(40) Gall, D.; Shin, C.-S.; Haasch, R. T.; Petrov, I.; Greene, J. E. Band Gap in Epitaxial NaCl-Structure CrN(001) Layers. *J. Appl. Phys.* **2002**, *91* (9), 5882−5886.
(41) Kerdsongpanya, S.; Sun, B.; Eriksson, F.; Jensen, J.; Lu, J.; Koh, Y. K.; Nong, N. V.; Balke, B.; Alling, B.; Eklund, P. Experimental and Theoretical Investigation of Cr1-xScxN Solid Solutions for Thermoelectrics. *J. Appl. Phys.* **2016**, *120* (21), No. 215103.
(42) Carle, M.; Pierrat, P.; Lahalle-Gravier, C.; Scherrer, S.; Scherrer, H. Transport Properties of N-Type Bi2(Te1−xSex)3 Single Crystal Solid Solutions ($x \leqslant 0.05$). *J. Phys. Chem. Solids* **1995**, *56* (2), 201−209.
(43) Papageorgiou, C.; Giapintzakis, J.; Kyratsi, T. Low Temperature Synthesis and Characterization of PbTe-Based Materials. *AIP Conf. Proc.* **2012**, *1449* (1), 135−138.
(44) Okuyama, T.; Sugiyama, T.; Tahashi, M.; Goto, H.; Natsume, T.; Takahashi, M. Synthesis and Characterization of Ca3Co4O9 Thermoelectric Ceramics Using the Slurry Sintering Method. *Electron. Commun. Jpn.* **2019**, *102* (1), 3−9.
(45) McGahay, M. E.; Khare, S. V.; Gall, D. Metal-Insulator Transitions in Epitaxial Rocksalt-Structure Cr1−x/2 N1−x Ox (001). *Phys. Rev. B* **2020**, *102* (23), No. 235102.


https://doi.org/10.1021/acsaem.4c01491
ACS Appl. Energy Mater. 2024, 7, 6785−6792